

SPECTRAL CONFUSION FOR COSMOLOGICAL SURVEYS OF REDSHIFTED CII EMISSION

A. KOGUT¹, E. DWEK¹, S. H. MOSELEY¹

Accepted by The Astrophysical Journal

ABSTRACT

Far infrared cooling lines are ubiquitous features in the spectra of star forming galaxies. Surveys of redshifted fine-structure lines provide a promising new tool to study structure formation and galactic evolution at redshifts including the epoch of reionization as well as the peak of star formation. Unlike neutral hydrogen surveys, where the 21 cm line is the only bright line, surveys of red-shifted fine-structure lines suffer from confusion generated by line broadening, spectral overlap of different lines, and the crowding of sources with redshift. We use simulations to investigate the resulting spectral confusion and derive observing parameters to minimize these effects in pencil-beam surveys of redshifted far-IR line emission. We generate simulated spectra of the 17 brightest far-IR lines in galaxies, covering the 150 to 1300 μm wavelength region corresponding to redshifts $0 < z < 7$, and develop a simple iterative algorithm that successfully identifies the 158 μm [CII] line and other lines. Although the [CII] line is a principal coolant for the interstellar medium, the assumption that the brightest observed lines in a given line of sight are always [CII] lines is a poor approximation to the simulated spectra once other lines are included. Blind line identification requires detection of fainter companion lines from the same host galaxies, driving survey sensitivity requirements. The observations require moderate spectral resolution $700 < R < 4000$ with angular resolution between $20''$ and $10'$, sufficiently narrow to minimize confusion yet sufficiently large to include a statistically meaningful number of sources.

Subject headings: cosmology: observations, methods: data analysis, galaxies: high redshift, line: identification

1. INTRODUCTION

Line emission or absorption is a promising probe of the high-redshift universe. Considerable theoretical and instrumental effort has been devoted to the use of the redshifted 21 cm line of neutral hydrogen in such a fashion (see Pritchard and Loeb (2012) for a recent review). Comparable observations using atomic or molecular lines at far-infrared wavelengths have seen less development. Recent advances in far-IR instrumentation, combining sensitive receivers with large collecting area, have led to the detection of far-IR lines in individual sources at cosmological distances, raising the prospects for a future generation of far-IR line surveys as a probe of the high-redshift universe.

Infrared fine structure lines are important coolants of the neutral and ionized gas phases of normal and starburst galaxies. They are easily excited, arise from the most abundant metals with low ionization potential, and are generally not affected by galactic or intergalactic attenuation. The strongest line is the $^2P_{3/2} \rightarrow ^2P_{1/2}$ fine-structure line of singly-ionized carbon at 157.74 μm rest wavelength. The ubiquity of carbon in the interstellar medium combined with the relatively low ionization potential and modest excitation temperature make the [CII] line bright, with as much as 0.1 – 1% of the total bolometric luminosity of the host galaxy emitted in this single line (Crawford et al. 1985; Stacey et al. 1991; Wright et al. 1991; Lord et al. 1996). The intrinsic line brightness and lack of significant attenuation from the galactic or intergalactic medium in the far infrared in turn render the [CII] line visible over cosmological

distances (Maiolino et al. 2005; Iono et al. 2006; Maiolino et al. 2009; Stacey et al. 2010; Ivison et al. 2010; Wagg et al. 2011; De Breuck et al. 2011; Venemans et al. 2012; Wagg et al. 2012; Neri et al. 2014; Riechers et al. 2014; De Breuck et al. 2014).

The ability to detect [CII] emission to redshifts $z > 7$ makes the [CII] line a promising candidate for cosmological surveys. [CII] emission originates from multiple phases of the interstellar medium. The combined emission from all phases serves as a marker for source redshift for surveys of large-scale structure (Gong et al. 2011; Uzgil et al. 2014). The empirical relation between [CII] and the bolometric far-IR luminosity allows the observed [CII] intensity to serve as a tracer of star-formation activity (De Looze et al. 2011, 2014; Herrera-Camus et al. 2014), while the ratio of [CII] to other far-IR lines probes physical conditions within different phases of interstellar medium of the host galaxies (Abel 2006; Cormier et al. 2012; Croxall et al. 2012; Kapala et al. 2014).

Several authors have discussed requirements for [CII] surveys at cosmological distances. da Cunha et al. (2013a) estimate that a 500-hour observation of the 2.4' diameter Hubble Deep Field with the Atacama Large Millimeter Array could yield 15 [CII] detections over the redshift range $1 < z < 6$. The sub-arcsecond angular resolution available for such interferometric observations minimizes confusion from source superposition within each synthesized beam, but the large number of independent pointings needed to map an area comparable to the HDF minimizes the integration time spent on any individual source so that only the brightest sources are detected.

Observations at coarser angular resolution reduce the need for multiple pointings, at the cost of introducing competing lines from foreground sources. Intensity map-

Alan.J.Kogut@nasa.gov

¹ Code 665, Goddard Space Flight Center, Greenbelt, MD 20771

ping is one such technique, using fluctuations in the spatial and spectral distribution of line emission from a superposition of sources to derive the underlying power spectrum of the individual, unresolved sources (see, *e.g.*, the discussion in Righi et al. (2008); Visbal and Loeb (2010); Gong et al. (2011)). Several such surveys have been proposed. For example, Uzgil et al. (2014) present a concept for [CII] intensity mapping using a 25-beam grating spectrometer each with beam width $10''$, while Silva et al. (2014) propose a suite of single-beam spectrometers each with $30''$ beam width.

The larger beam size anticipated for such surveys facilitates mapping large areas but requires additional analysis to separate the target line emission from the foreground created by emission from other galaxies along the same line of sight. Several authors discuss cross-correlation techniques to minimize foreground confusion in line intensity mapping (Righi et al. 2008; Visbal and Loeb 2010). For a given target redshift, the technique defines two observing wavelengths corresponding to emission from two different rest-frame lines. Maps of line emission taken at each observing wavelength contain spatially correlated structure corresponding to the two lines emitted by each source galaxy. The contribution from other lines at different rest-frame wavelengths redshifted into the observing wavelengths must originate from sources at different redshifts. Spatial correlations from such distant sources will be weaker, so that the cross-correlation traces the power spectrum of the source galaxies at the target redshift.

Intensity mapping surveys large volumes of the universe to derive statistical estimates of structure formation, but provides little information on individual sources. In this paper, we investigate the complementary technique of direct line identification in narrow-beam spectroscopic surveys. If the [CII] line were the only observable far-IR line, redshift identification would be straightforward. In practice, however, the [CII] line is merely one of several cooling lines. The problem of sorting through an observed spectrum containing multiple lines from multiple galaxies at different redshifts presents both instrumental and analytical challenges. We use a toy model of far-IR line emission to evaluate a simple algorithm for line identification and estimate relevant instrumental parameters (angular resolution, sensitivity, and spectroscopic resolution) required to derive cosmologically interesting results. The results are applicable for spectral cleaning of intensity mapping surveys as well as pencil-beam surveys of more limited cosmological volume.

2. METHODOLOGY

We use a simple model of the brightest far-IR lines to simulate the observed line spectra from distant galaxies. We assume that the total luminosity, $\ell(\nu_0)$ emitted in a single line at rest frequency ν_0 may be simply related to the total infrared luminosity, L_{IR} of a galaxy,

$$\ell(\nu) = f(\nu_0, L_{IR}) L_{IR}. \quad (1)$$

The observed specific flux of a single line from a set of IR galaxies at redshift z is then given by

$$F_\nu(\nu, z) = (1+z) \frac{dV_c(z)}{4\pi d_L^2(z)} \quad (2)$$

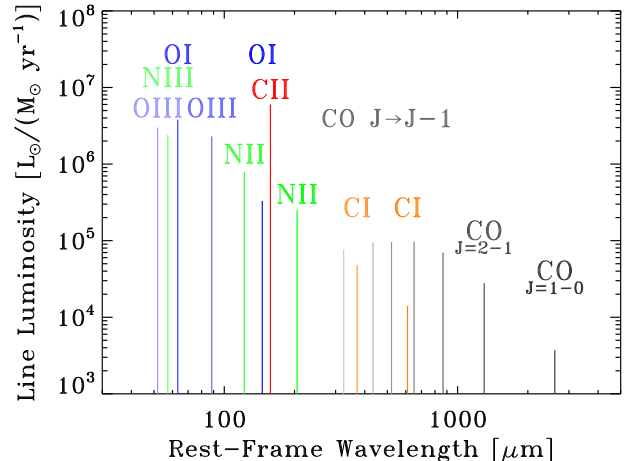


FIG. 1.— Rest-frame wavelength and mean relative luminosity for the far-IR lines used in this study (see Table 1 in Visbal, Trac, and Loeb (2011)).

$$\times \int_{L_1}^{L_2} dL_{IR} \Phi(L_{IR}, z) f(\nu_0, L_{IR}) \phi_\nu(\nu')$$

where $\Phi(L_{IR}, z)$ is the galaxy IR luminosity function, $d_L(z)$ is the luminosity distance, $\nu' = \nu(1+z)$ is the redshifted frequency, and $\phi_\nu(\nu)$ is the intrinsic line profile, normalized so that $\int \phi_\nu(\nu) d\nu = 1$. Ignoring the effects of gravitational lensing, the total line intensity emitted from galaxies within a redshift interval z_0 to the present ($z = 0$) then becomes

$$F_\nu(\nu) = \frac{\Omega}{4\pi} \int_0^{z_1} \left| \frac{cdt}{dz} \right| \frac{dz}{1+z} \times \left[\int_{L_1}^{L_2} dL_{IR} \Phi(L_{IR}, z) f(\nu_0, L_{IR}) \phi_\nu(\nu') \right] \quad (3)$$

If the ratio of line intensity to IR luminosity is a constant, Eq. (3) simplifies to

$$F_\nu(\nu) = \frac{\Omega}{4\pi} f(\nu_0) L_\star \int_0^{z_1} n(z) \phi_\nu[\nu(1+z)] \left| \frac{cdt}{dz} \right| \frac{dz}{1+z} \quad (4)$$

where

$$\int_{L_1}^{L_2} \Phi(L_{IR}, z) dL_{IR} = n(z) L_\star, \quad (5)$$

$n(z)$ is the comoving number density of galaxies, and

$$L_\star \equiv \frac{\int L \Phi(L) dL}{\int \Phi(L) dL} \quad (6)$$

is their average IR luminosity.

We simulate the far-IR line spectra using a standard cosmology with $h = 0.7$, $\Omega_m = 0.28$, and $\Omega_\Lambda = 0.72$ (Hinshaw et al. 2013). We divide the comoving volume into redshift bins and compute the total number of galaxies $N(z)$ within each bin

$$\frac{dN(z)}{dz} = n(z) \frac{dV_c(z)}{dz} \quad (7)$$

where $V_c(z)$ is the comoving volume at redshift z . We use the resulting number density to generate Monte Carlo re-

alizations of the far-IR line spectra. The background cosmology fixes the mean number of galaxies within a fixed observing solid angle. We assign each simulated galaxy a redshift and IR luminosity, using the Saunders et al. (1990) luminosity function to obtain a representative luminosity distribution within each redshift bin.

Each galaxy then contributes a set of far-IR lines. Figure 1 shows the relative intensity of the rest-frame lines used for this study. We include the [CII] line at 158 μm , [CI] at 610 and 371 μm , [OIII] at 88 and 52 μm , [OI] at 145 and 63 μm , [NIII] at 57 μm , and [NII] at 205 and 122 μm , as well as the CO ($J \rightarrow J-1$) series through $J=7$. The total luminosity in each line is related to that of the host galaxy by the factor $f(\nu_0)$ (Eq. 1). We set the mean value of f for each line using the ratios of values in Table 1 of Visbal, Trac, and Loeb (2011). For simplicity, we do not explicitly calculate the star formation rate for each simulated galaxy, but relate the comoving star formation rate $\dot{\rho}(z)$ to the IR luminosity density $\mathcal{L}(z)$ as

$$\mathcal{L}(z) \approx \mathcal{A}\dot{\rho}(z) \quad (8)$$

where $\mathcal{L}(z)$ is the comoving IR luminosity density, $\dot{\rho}(z)$ is the comoving cosmic star formation rate (CSFR) in $M_\odot \text{ yr}^{-1} \text{ Mpc}^{-3}$, and $\mathcal{A} = 6.7 \times 10^9$ is a conversion factor for a Salpeter stellar initial mass function (Kennicutt 2012).

The relative luminosities from different lines within a source are known to vary by roughly a factor of 10. We account for such variation by multiplying $f(\nu_0)$ for each line in each host galaxy by a random number drawn uniformly from the range [0.3 – 3]. We additionally account for the systematic variation in line luminosity and line ratios due to the increased CMB temperature at higher redshift (da Cunha et al. 2013b). We assume that the host galaxies are not spatially resolved and assign a random rotational linewidth to each galaxy uniformly drawn from the range [30 – 300] km s^{-1} . Each galaxy contributes multiple lines; all lines from a single galaxy have the same rotational line broadening. Finally, we accumulate the lines from all source galaxies within the sampled volume and redshift each line to obtain a realization the observed far-IR spectrum. The effects of instrument spectroscopic resolution are discussed in §3.2. We ignore instrument noise and continuum emission from the superposed host galaxies to focus here on the problem of line identification.

Figure 2 shows a typical spectrum with $2'$ angular resolution at wavelengths corresponding to redshifts $4.4 < z < 4.5$ for the [CII] line. Two problems are evident. The first problem is confusion. Unlike radio observations, where the redshifted 21 cm line is the only bright line, a number of lines contribute to the observed far-IR spectra. Only 16% of the lines within the observed wavelength range correspond to the targeted [CII] line, with the remainder consisting of “interloper” lines originating at both higher and lower redshifts from species other than [CII]. The second problem is blending: the superposition of rotationally broadened lines produces a complicated spectrum. The fainter lines merge to form a near continuum spectrum, further hindering line identification.

3. LINE IDENTIFICATION

Although the [CII] line is bright, simply assuming that the brightest observed lines within a single field are always [CII] lines produces a high error rate for line identification. We quantify this by taking the simulated spectra and selecting the brightest 10% of lines within a narrow range centered at different source redshifts. We may then count how many of the brightest lines in each range are in fact [CII] lines as opposed to interloper lines from sources at other redshifts. The probability that a given line within the brightest 10% is in fact a [CII] line falls from 0.8 for observations near 315 μm ($z_s = 1$) to 0.4 for observations at 1100 μm ($z_s = 6$).

We address the problem of blind line identification using a version of the radio-astronomical CLEAN algorithm. Although the brightest lines are not necessarily [CII] lines, the [CII] lines are generally bright. This suggests an iterative process. We first select the brightest line within the observed spectrum. Assuming that this “parent” line is [CII] fixes the corresponding source redshift z_s . We then predict the wavelengths at which other far-IR lines originating from the same source should be

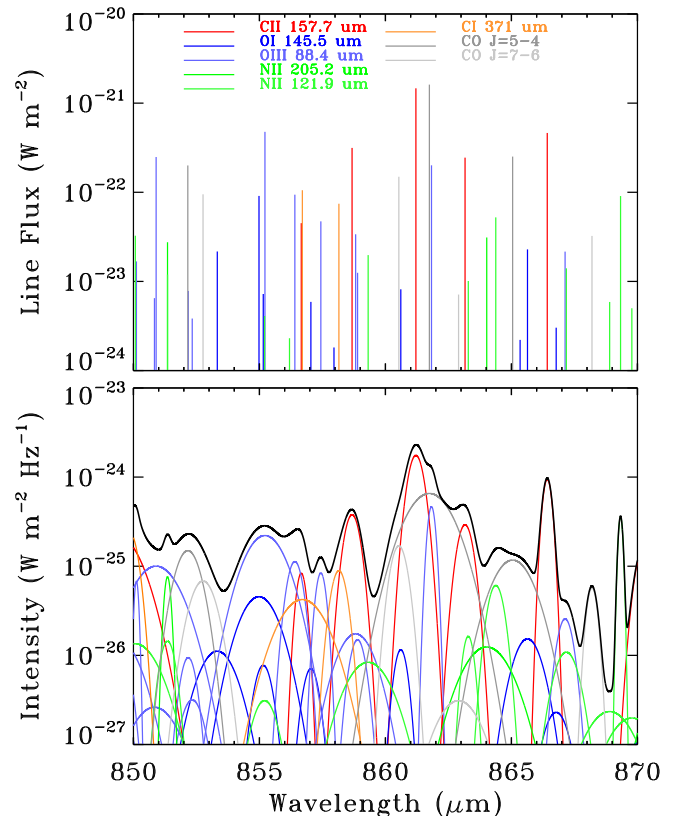


FIG. 2.— Simulated spectrum with red-shifted lines. The wavelength range corresponds to redshift $4.4 < z < 4.5$ for the [CII] line. (Top) Individual line flux, shown at the central wavelength before rotational broadening. Lines are color-coded by species using the same color coding as Figure 1. 48 lines from 48 individual galaxies at $0.6 < z < 8$ fall within the plotted wavelength range. The assumption that the brightest lines are always [CII] lines produces a high error rate, with roughly a third of the brightest lines originating from species other than [CII]. (Bottom) The same lines are shown after rotational broadening. The superposition of rotationally broadened lines produces a complicated spectrum (black curve).

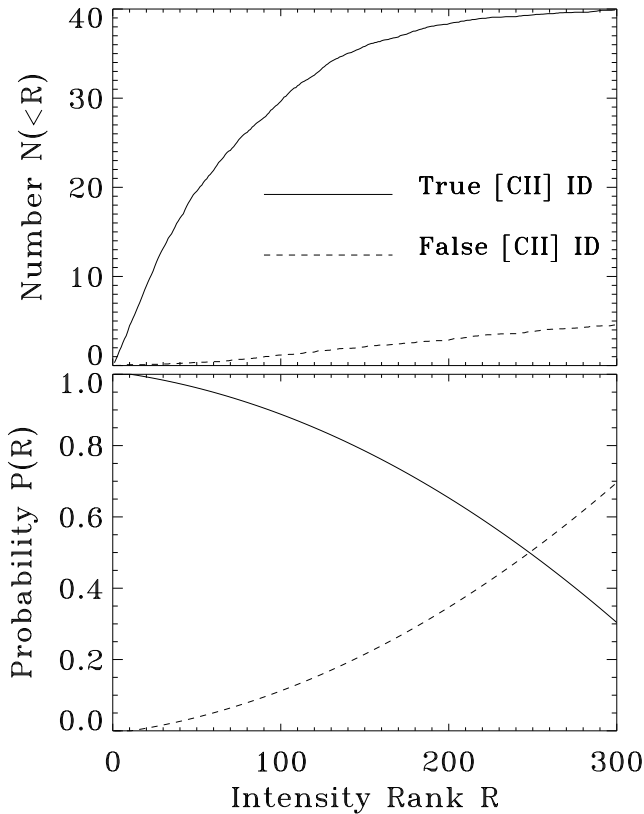


FIG. 3.— Results of the CLEAN algorithm compared to simulation inputs for a simulated spectrum from $580 \mu\text{m}$ to $1160 \mu\text{m}$ containing 390 peaks (see text). (Top) Cumulative number of correct (solid line) and incorrect (dashed) [CII] line identifications as a function of the relative line intensity, sorted from brightest ($R = 0$) to faintest ($R = 300$). (Bottom) Probability that the R^{th} -brightest peak in the observed spectra will be correctly identified. The number of false identifications is small for the brightest half of the observed lines.

observed,

$$\lambda_{\text{pred}} = \lambda_{\text{rest}} (1 + z_s), \quad (9)$$

and examine the spectra at those wavelengths. If the expected “companion” lines are found, the redshift identification is confirmed and both the candidate [CII] line and the detected companion lines are flagged as known and removed from the list of lines to search. If no companion lines are found, we repeat the test assuming that the parent line is the next-most-common far-IR line (typically a CO line) and continue down the list of far-IR lines until we identify a parent/companion combination or exhaust the list of potential parent lines. If no companion lines are found, the bright parent line is flagged as unknown and removed from the list of possible parent lines, although it may later be identified as a companion line. We then proceed to the brightest remaining un-flagged line and iterate until all lines are tested.

3.1. Efficiency and Error Rate

We test the algorithm using Monte Carlo realizations of the observed spectra and compare the derived identifications to the known Monte Carlo inputs to determine the detection efficiency and error rate. Figure 3 shows the results obtained from a single $2'$ beam observing one octave

in wavelength from $580 \mu\text{m}$ to $1160 \mu\text{m}$, corresponding to [CII] redshifts $2.7 < z_s < 6.3$. The input spectrum contains 1600 spectral lines from 550 distinct galaxies, including 260 [CII] lines. After rotational broadening, the observed superposed spectrum contains 390 peaks², 110 of which result from a [CII] line. Blending is significant: of the 390 peaks in the superposed spectra, 290 are dominated by a single line and 100 are blends of multiple lines. The un-blended peaks comprise 175 unique host galaxies.

The line identification algorithm starts with the brightest such peak and works to progressively fainter peaks. The algorithm correctly identifies 200 lines corresponding to 80 unique parent redshifts and 120 companion lines. 40 of the correctly identified parent lines result from [CII] emission, with the remainder primarily from lower-redshift CO lines. The detection efficiency is thus 15% of the 260 [CII] lines input to the simulation, or 36% of the 110 potentially detectable [CII] lines in the superposed spectra.

The algorithm correctly identifies half of the 390 peaks in the superposed spectra. The remaining 190 peaks are either incorrectly identified (160 peaks) or not identified (30 peaks). False identifications typically result from blended lines and are spread uniformly across all 17 candidate lines (i.e. with 5–10 false identifications for each line in Figure 1). The error rate is a function of relative line intensity, with the probability of a correct identification near unity for the brightest 10–15 lines and remaining above 75% for lines in the brightest half of the observed spectrum (30–40 lines for the parameters in Figure 3). Lines in the faintest third of the observable spectrum are more likely to generate a false identification than a true identification. Restricting the algorithm to searching only the brightest half of the observed set of lines reduces the number of correctly-identified [CII] lines from 40 to 38 while yielding only 3 false identifications, for an error rate of 7%.

Incorrect line identification results from the chance spectral alignment of one line from one galaxy with a different line from a different galaxy. The spectral density of lines increases at fainter intensities (Fig 2), increasing the probability for such alignment. Restricting potential “parent” lines to the brightest half of observed lines largely eliminates this problem without sacrificing correct identifications. Incorrectly identified lines may also be flagged through anomalous line ratios, although in this work we do not apply such a line ratio test.

3.2. Spectral Resolution

The CLEAN algorithm identifies [CII] lines by searching for predicted “companion” lines among the set of observed spectral lines. As the number of lines increases, confusion from overlapping or blended lines can create errors in the position of the fitted line centers to limit the efficiency of the algorithm. We use simulated spectra to assess the instrumental parameters required to mitigate line confusion.

The number of lines depends on the number of galaxies within a spatially unresolved observation. Decreas-

² Working with noiseless simulations, we define a “peak” as any spectral bin brighter than two neighbors on either side. The effects of coarser instrumental resolution are discussed in § 3.2

ing the angular resolution increases both the number of galaxies observed and the spectral density of emission lines. Observing more spectral lines in turn increases the probability that lines from different source redshifts will overlap in wavelength, requiring higher spectral resolution to distinguish individual lines.

We quantify the spectroscopic resolution as a function of the angular resolution. For a given angular resolution, we simulate the galaxy population and generate the superposed spectra (including rotational broadening) from all sources using the species in Figure 1. We identify all peaks in the resulting (noiseless) spectra and compare the separation $\Delta\lambda$ between adjacent peaks to the wavelength λ to determine the spectral resolution $R = \lambda/\Delta\lambda$ needed to distinguish the two as separate lines.

Figure 4 shows the fraction of the observed spectral peaks whose separation $\Delta\lambda$ from the neighboring peak is greater than $2\lambda/R$, where the factor of 2 accounts for the need to observe two distinct peaks. At low spectral resolution, the lines are heavily blended so that only the few brightest lines can be distinguished. As the instrument spectral resolution increases, progressively more of the lines can be distinguished. The spectral resolution needed to distinguish separate peaks depends on the angular resolution: decreasing the angular resolution reduces the number of galaxies observed, producing correspondingly greater separation between adjacent peaks in the observed spectra. Spectral resolution $R = 700$ (velocity resolution 430 km s^{-1}) successfully resolves 90% of the peaks in the blended spectra for a $20''$ resolution. A higher resolution $R = 4000$ (75 km s^{-1}) is required to resolve 90% of the peaks for $10'$ resolution. Rotational line widths of a few hundred km s^{-1} effectively limit the resolution to values $R < 5000$ independent of the angular resolution. Increasing the spectral resolution above $R = 5000$ does not distinguish additional lines, as the observed spectra are then limited

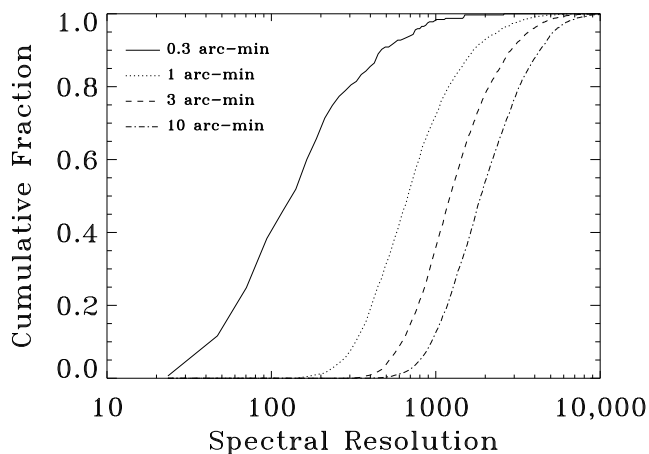


FIG. 4.— Fraction of adjacent peaks in the simulated spectra that can be resolved at spectral resolution R . Results are shown for angular resolution 0.3, 1, 3, and 10 arc-minutes (left to right). Observations at modest spectral resolution ($R \sim 3000$) resolve as much of the blended spectrum as possible. The superposition of rotationally broadened lines from multiple sources creates an effective ceiling at $R \sim 5000$. Observations at higher spectral resolution do not distinguish additional lines.

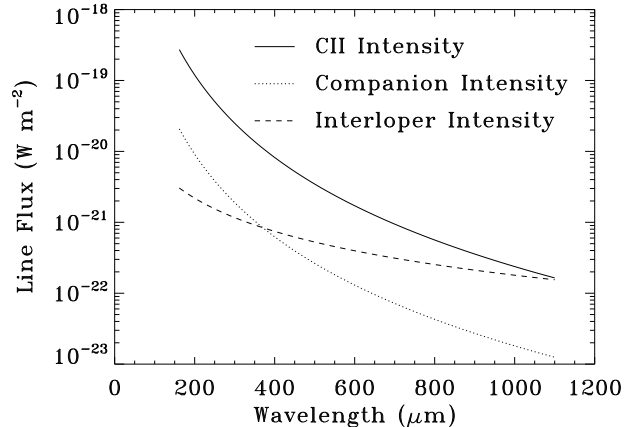


FIG. 5.— Flux from the red-shifted [CII] line (solid line) as a function of observing wavelength. The mean flux of the brighter companion lines from each [CII] source is shown as a dotted line, while the dashed line shows the flux of competing emission from unrelated interloper lines.

by intrinsic source blending and not by the instrument.

3.3. Sensitivity

The line identification algorithm requires sufficient instrumental sensitivity to detect both the [CII] line as well as one or more companion lines. Figure 5 shows the typical line flux as a function of observing wavelength. For each [CII] source in the simulation, we compute the [CII] line intensity as well as the mean intensity of the four companion lines ([OI] $146 \mu\text{m}$, [OIII] $88 \mu\text{m}$, [NII] $205 \mu\text{m}$, and [NII] $122 \mu\text{m}$) most often used by the algorithm for successful [CII] identifications. To the extent that physical conditions in the interstellar medium remain constant, the ratio of companion to [CII] line intensity remains constant so that the observed line fluxes simply fall at the longer observing wavelengths in accordance with the higher source redshift. Interloper lines, however, include sources at multiple redshifts unrelated to the [CII] source redshift and thus fall more slowly with wavelength.

The companion lines are roughly a factor of 10 fainter than the [CII] line. Observations using the CLEAN algorithm to determine source redshift must retain sufficient sensitivity to observe these fainter companion lines in addition to the targeted [CII] lines. Interloper lines become brighter than the companion lines for wavelengths $\lambda > 350 \mu\text{m}$ corresponding to [CII] source redshift $z_s > 1$. Observations at longer wavelengths targeting higher source redshifts require sufficient spectral resolution to distinguish the companion lines from the brighter interloper lines (Figure 4).

The requirement to distinguish at least one identifiable companion line for each [CII] line implies that the sensitivity and integration times for a blind survey are determined by the fainter companion lines and not the targeted [CII] lines. To reduce the total observing time needed to map a given field, surveys are likely to employ multiple spectrometers simultaneously observing independent lines of sight. Such an arrangement has been envisioned for future surveys Silva et al. (2014); Uzgil et al. (2014)

4. PENCIL-BEAM SURVEY

The ubiquity and intensity of line emission from ionized carbon makes the [CII] line a promising probe of the high-redshift universe. We may thus anticipate future surveys using the [CII] line for redshifts $z < 10$ to probe large scale structure, galaxy evolution, and the epoch of reionization (Suginohara et al. 1999; Righi et al. 2008; Visbal, Trac, and Loeb 2011; Gong et al. 2012; Silva et al. 2014; Uzgil et al. 2014). Instrumental requirements for such a survey, however, are not clear. Observations from ground-based platforms (e.g. ALMA or PdBI) allow large collecting areas but are limited to the available atmospheric windows. Even within these windows, atmospheric emission is 6 orders of magnitude brighter than the astrophysical foregrounds. The resulting photon noise limits sensitivity, requiring integration times of 500 hours to detect a handful of sources within a cosmologically interesting volume (da Cunha et al. 2013a).

Observations from a balloon or space platform can mitigate atmospheric emission at the cost of limiting the size of the beam-forming optics. The smaller collecting area reduces sensitivity to individual unresolved sources, while the coarser angular resolution increases confusion from multiple sources within each angular resolution element. Uzgil et al. (2014) discuss intensity mapping from a balloon platform as one way to cope with these problems. Here we consider the complementary approach of a pencil-beam survey from a small millimeter-wave telescope. A pencil-beam survey allows a single instrument to measure multiple galaxies within each line of sight, using spectroscopy to separate individual sources and determine source redshifts.

Figure 6 shows the number of [CII] lines that could be identified within a single pointing for a noiseless instrument. We simulate a single $2'$ beam observed with spectral resolution $R = 3000$ over one octave in wavelength and use the CLEAN algorithm to identify lines within the resulting spectra. We examine 3 cases for spectral bands 300–600 μm , 500–1000 μm , and 700–1400 μm corresponding to targeted [CII] redshifts $z = 2, 4,$ and 6 . The upper panel shows the cumulative number count $N(> S)$ for all [CII] lines brighter than threshold S that were identified by the algorithm. The broad spectral band allows the number counts to include sources over a range of redshifts. The bottom panel shows the number counts for the subset of detected lines within 20% of the target redshift. A single pointing at 5σ threshold of 0.3 mJy can potentially identify 20–40 redshifted [CII] lines (plus a comparable number of companion lines) within a $2'$ beam.

We illustrate the potential utility of a pencil-beam survey using a toy model of the star formation history. We compare a model with no luminosity evolution to a second model for which the typical luminosity increases by a factor of 5 at redshift z_p . Figure 7 shows the result. The recovered luminosity distributions accurately reflect the toy model luminosity evolution. Such a pencil-beam survey easily distinguishes a model in which the luminosity peaks at $z_p \sim 2.5$ from a model with no evolution.

5. CONCLUSIONS

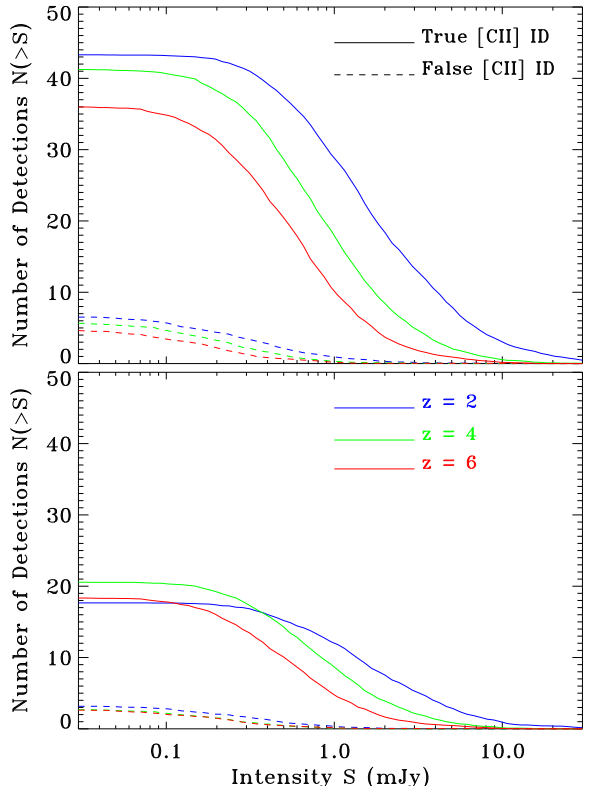


FIG. 6.— Number of identified [CII] lines as a function of line intensity. Solid lines show the cumulative [CII] number counts derived from simulations of a single $2'$ beam observed over one octave in wavelength centered at redshifts 2 (top curve, blue), 4 (green), or 6 (bottom curve, red). Dashed lines show the number of false identifications. Companion lines are not shown. (Top) Total number of [CII] detections over the full wavelength band. (Bottom) Subset of detected lines with redshift lying within 20% of the target redshift.

The [CII] line is a principal coolant of the interstellar medium and is observable at cosmological distances. However, the [CII] line is observed against a forest of competing lines from sources at multiple redshifts. We use Monte Carlo simulations of the galaxy distribution at redshifts $0 < z < 9$ to generate realizations of the far-IR spectra including emission from 17 of the brightest far-IR lines. The resulting spectra provide a test bed to evaluate the use of the [CII] line as a cosmological probe in blind pencil-beam surveys.

The superposition of rotationally-broadened lines from multiple galaxies at different redshifts creates a complex spectrum. The simplest assumption, that the brightest lines are always [CII] lines, is at best a coarse approximation to the simulated spectra. The fraction of [CII] lines among the brightest 10% of all observed lines falls from 0.8 for observations near 315 μm ($z_s = 1$) to 0.4 at 1100 μm ($z_s = 6$). Line identification based solely on relative intensity produces a high error rate.

A variant of the radio-astronomical CLEAN algorithm yields superior results. The algorithm selects the brightest line from an observed set of spectral lines, tentatively identifies the line as [CII], and uses the resulting source redshift to predict the observed wavelengths for redshifted line emission from other bright far-IR lines

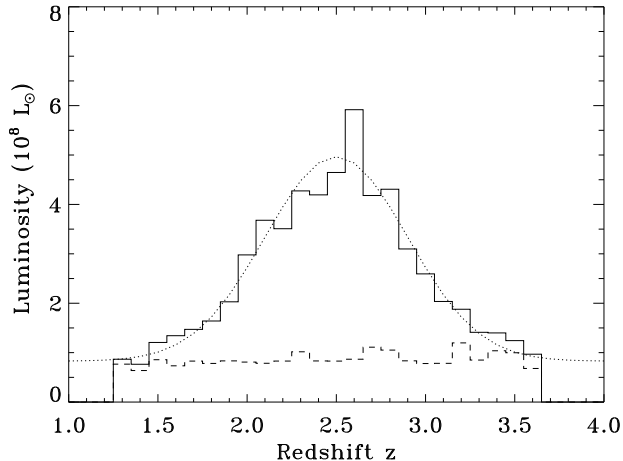


FIG. 7.— Galaxy luminosity distribution derived from a simulated pencil-beam survey observing the [C II] line over one octave in wavelength at spectral resolution $R = 3000$. The recovered luminosity distribution (solid line) accurately follows the toy model (dotted curve). The dashed line shows the recovered luminosity distribution for a model without luminosity evolution.

from the same source. If the predicted lines are observed, the source identification is confirmed and the [CII] line and redshifted companion lines are flagged and removed from the list of unknown lines. If the predicted lines are not observed, the source identification is not confirmed and the bright source line remains on the list of unknown lines for possible later identification as a companion line for a source at a different redshift. The algorithm then proceeds to the next brightest remaining line and iterates until all lines have been processed.

A typical spectrum for $2'$ angular resolution contains some 1600 spectral lines within one octave, originating from 550 different galaxies. The superposition of rotationally broadened lines reduces this to roughly 390 distinct peaks in the observed spectrum, 110 of which result from a single un-blended [CII] line. The line identification algorithm correctly identifies 40 of the 110 [CII]

line peaks for an efficiency of order 36% (not counting companion lines identified from the same host galaxies). Chance alignments of lines lead the algorithm to incorrectly identify 3 peaks as [CII] lines; however, the incorrect identifications result almost exclusively from fainter candidate peaks. Restricting the algorithm to the brightest third of the observed peaks (corresponding roughly to threshold 0.3 mJy) increases the percentage of correct identifications above 90%. Correct line identification requires detection of both the targeted “parent” line and one or more “companion” lines from the same source. Survey sensitivity thresholds are thus determined by the expected intensities of the companion lines and not solely by the brighter [CII] line.

The ability to distinguish individual peaks in the superposed spectra depends on the spectral resolution and angular resolution. Decreasing the angular resolution increases the number of lines in the observed spectra, requiring higher spectral resolution to minimize blending of neighboring lines. The required resolutions are modest. Spectral resolution $R = 700$ resolves 90% of the peaks for $20''$ angular resolution, while $R = 4000$ resolves 90% of the peaks for $10'$ angular resolution or coarser.

The [CII] line is a promising cosmological probe. The large number of potential sources observed within a single pencil beam combined with an efficient and accurate line identification algorithm allow rapid characterization of the galaxy luminosity distribution to redshifts encompassing reionization. A simulated pencil-beam survey demonstrates the ability to distinguish toy models of galaxy evolution within a single angular resolution element. The required angular resolution, sensitivity, wavelength range, and spectroscopic resolution appear achievable, suggesting that far-IR lines may soon provide a new tool to map the large-scale galaxy distribution and evolution for redshifts $0 < z_s < 10$.

We thank D. Leisawitz for encouraging development of the simulations. Support for this research came from NASA’s Science Innovation Fund.

REFERENCES

- Abel, N. P., 2006, MNRAS, 368, 1949
 Crawford, K. M., et al., 1985, ApJ, 291, 755
 Cormier, D., et al., 2012, A&A, 548, A20
 Croxall, K. V., et al., 2012, ApJ, 747, 81
 da Cunha, E., et al., 2013, ApJ, 765, 9
 da Cunha, E., et al., 2013, ApJ, 766, 13
 De Breuck, C., et al., 2011, A&A, L8
 De Breuck, C., et al., 2014, A&A, 565, A59
 de Looze, I., et al., 2011, MNRAS, 416, 2712
 de Looze, I., et al., 2014, A&A, 568, A62
 Gong, Y., et al., 2011, ApJ, 728, L46
 Gong, Y., et al., 2012, ApJ, 745, 49
 Herrera-Camus, R., et al., 2014, arXiv:1409.7123
 Hinshaw, G., et al., 2013, ApJS, 208, 19
 Iono, D., et al., 2006, ApJ, 645, L97
 Ivison, R. J., et al., 2010, A&A, 518, L35
 Kapala, M. J., et al., 2014, arXiv:1410.6158
 Lord, S.D., et al., 1996, A&A, 315, L117
 Maiolino, R., et al., 2005, A&A, 440, L51
 Maiolino, R., et al., 2009, A&A, 500, L1
 Neri, R., et al., 2014, A&A, 562, A35
 Pritchard, J. R., and Loeb, A., 2012, Rep. Prog. Phys., 75, 086901
 Riechers, D. A., et al., 2014, ApJ, 796, 84
 Righi, M., Hernandez-Monteagudo, C., and Sunyaev, R. A., 2008, A&A, 489, 489
 Saunders, W., et al., 1990, MNRAS, 242, 318
 Silva, M., Santos, M. G., Cooray, A., and Gong, Y., 2014, arXiv:1410.4808
 Stacey, G. J., et al., 1991, ApJ, 373, 423
 Stacey, G. J., et al., 2010, ApJ, 724, 957
 Sugihara, M., Sugihara, T., and Spergel, D. N., 1999, ApJ, 512, 547
 Uzgil, B. D., et al., 2014, ApJ, 793, 116
 Venemans, B. P., et al., 2012, ApJ, 751, L25
 Visbal, E., and Loeb, A., 2010, JCAP, 11, 16
 Visbal, E., Trac, H., and Loeb, A., 2011, JCAP, 8, 10
 Wagg, J., et al., 2011, A&A, 519, L1
 Wagg, J., et al., 2012, ApJ, 752, L30
 Wright, E. L., et al., 1991, ApJ, 381, 200